

# TeV black hole fragmentation and detectability in extensive air showers

Eun-Joo Ahn\*

*Department of Astronomy & Astrophysics, University of Chicago,  
5640 S. Ellis Avenue, Chicago, IL 60637, USA*

Maximo Ave†

*Enrico Fermi Institute, University of Chicago,  
5640 S. Ellis Avenue, Chicago, IL 60637, USA*

Marco Cavaglia‡

*Institute of Cosmology and Gravitation,  
University of Portsmouth, Portsmouth PO1 2EG, UK*

Angela V. Olinto§

*Department of Astronomy & Astrophysics, Enrico Fermi Institute,  
and Center for Cosmological Physics, University of Chicago,  
5640 S. Ellis Avenue, Chicago, IL 60637, USA*

(Dated: December 3, 2021)

## Abstract

In models with large extra dimensions, particle collisions with center-of-mass energy larger than the fundamental gravitational scale can generate nonperturbative gravitational objects. Since cosmic rays have been observed with energies above  $10^8$  TeV, gravitational effects in the TeV energy range can, in principle, be observed by ultrahigh energy cosmic ray detectors. We consider the interaction of ultrahigh energy neutrinos in the atmosphere and compare extensive air showers from TeV black hole formation and fragmentation with standard model processes. Departures from the standard model predictions arise in the interaction cross sections and in the multiplicity of secondary particles. Large theoretical uncertainties in the black hole cross section weaken attempts to constrain TeV gravity based solely on differences between predicted and observed event rates. The large multiplicity of secondaries in black hole fragmentation enhances the detectability of TeV gravity effects. We simulate TeV black hole air showers using PYTHIA and AIRES, and find that black hole-induced air showers are quite distinct from standard model air showers. However, the limited amount of information registered by realistic detectors together with large air shower fluctuations limit in practice the ability to distinguish TeV gravity events from standard model events in a shower by shower case. We discuss possible strategies to optimize the detectability of black hole events and propose a few unique signatures that may allow future high statistics detectors to separate black hole from standard model events.

PACS numbers: 96.40.-z, 96.40.Tv, 95.85.Ry, 04.50.+h, 04.70.-s, 04.80.Cc

---

\*Email: sein@oddjob.uchicago.edu

†Email: ave@cfcf.uchicago.edu

‡Email: marco.cavaglia@port.ac.uk

§Email: olinto@oddjob.uchicago.edu

## I. INTRODUCTION

In models with large extra dimensions, the fundamental scale of gravity may be around TeV energies [1, 2, 3, 4, 5]. The presence of extra dimensions affects both sub- and super-Planckian physics. Sub-Planckian physics is affected by the presence of Kaluza-Klein modes that lead to deviations from standard model (SM) predictions in perturbative processes [6, 7, 8, 9]. Searches for these effects in collider experiments have placed bounds on the fundamental Planck scale,  $M_\star \geq 1.3$  TeV for two extra dimensions and  $M_\star \geq 0.25$  TeV for six extra dimensions [10]. Additionally, submillimeter tests of the gravitational inverse-square law constrain  $M_\star \geq 1.6$  TeV for  $n = 2$  [11].

Super-Planckian physics involves nonperturbative effects, the most striking being the possible formation of black holes (BHs) [12] and other gravitational objects [13, 14, 15, 16, 17] in particle collisions with center-of-mass (CM) energy larger than the fundamental Planck scale. (For recent reviews, see Refs. [18, 19, 20, 21].) If the fundamental scale is of the order of a few TeV, the products of BH decay could be detected in particle colliders [22, 23, 24, 25] and in extensive air showers of ultrahigh energies [26, 27, 28, 29, 30, 31].

Ultrahigh energy cosmic rays provide a natural beam of particles with primary energies up to and above  $10^8$  TeV that can in principle probe TeV scale physics. The dominant component of ultrahigh energy cosmic rays (UHECRs) is believed to be protons [32] generated in extra-galactic sources. UHECR protons naturally generate ultrahigh energy neutrinos as they traverse intergalactic space through photo-pion production off the cosmic microwave background (CMB) [33, 34]. The threshold energy for pion production off the CMB induces a feature in the UHECR spectrum known as the Greisen, Zatsepin, and Kuzmin (GZK) feature [35, 36]. The flux of neutrino secondaries from the pion production depends on the assumed extra-galactic proton injection spectrum and generally peaks around  $10^6$  TeV [33, 34, 37, 38]. These secondary neutrinos are often called GZK or cosmogenic neutrinos. Here we study the characteristics of extensive air showers initiated by ultrahigh energy neutrinos and compare the production of BHs in TeV gravity theories with SM interactions.

Ultrahigh energy neutrinos provide a useful means to test TeV gravity. In some TeV gravity models, the neutrino-nucleon cross section,  $\sigma_{\nu N}$ , is greatly enhanced, leading to larger numbers of neutrino-induced air shower events. In fact, the lack of observed neutrino air showers can be used to place a bound on the neutrino-nucleon cross section that has been

translated into constraints on  $M_\star$  comparable to collider limits [28, 39]. However, the physics of BH formation and evolution in TeV gravity theories is highly uncertain and model dependent. As we discuss below, the cross section of the process can only be roughly estimated. While some choices of parameters lead to the enhancement of neutrino-nucleon cross sections compared to the SM, others choices give cross sections for BH formation orders of magnitude below the SM case. Furthermore, the evaporation process of BHs generates additional uncertainties on the fraction of the primary energy that is left to generate a shower. Even if a limit on the neutrino cross-section can be derived from the lack of neutrino-induced air showers (for example, if the cosmogenic neutrino flux is better constrained), translating a bound on  $\sigma_{\nu N}$  into a limit on TeV gravity parameters is highly model dependent. Therefore, the identification of quantum gravity effects based solely on neutrino event rates is not very effective.

Here we take a different approach by modeling the detailed characteristics of extensive air showers initiated by BH evaporation on a shower-to-shower basis, with the expectation that the large multiplicity of secondaries will lead to detectable signatures. We first calculate the fragmentation of BH and the spectrum of secondaries. The secondary particles are then developed with PYTHIA [40] and AIRES [41] into observable extensive air showers. We find that BH-induced air showers generally differ from ordinary air showers. Differences in shower maxima reach  $\sim 200 \text{ g cm}^{-2}$  between BH and SM events which could be easily detected if the first interaction point of the air showers were either observed or fixed by the interaction. Unfortunately, the first interaction point of high energy neutrinos in the atmosphere is neither fixed by the interaction nor detectable. Unlike protons, the interaction length of neutrinos in air is quite large, thus neutrinos interact with almost equal probability at any point in the atmosphere. Moreover, the first interaction point is not directly observed since fluorescence experiments can only detect the air shower once billions of particles have been generated while ground arrays only observe the air shower as it reaches the ground. Shower observables such as the muon content and the rise-depth parameter give indirect signatures that can distinguish BH and SM events in large statistics experiments that combine fluorescence detectors and ground array detectors.

In addition to differences in the overall characteristics of air showers, BH formation produces some unique signatures since the fragmentation secondaries span most particles in the SM. In particular, heavy BHs may produce several  $\tau$ -leptons. Multiple  $\tau$ 's are unique

to BH formation and may be differentiated in future UHECR observatories.

The paper is organized as follows. In the first part of §II, we review BH formation in TeV gravity and the physics of the BH-induced atmospheric events. The aim of this part is to fix notations and make the paper self-consistent. In the second part of §II we first focus on the cross section uncertainties, which make the identification of atmospheric BH formation based solely on event rates ineffective. Next we discuss the phenomenology of BH evaporation, which is the backbone of the air shower simulations. In §III, we describe the Monte Carlo that we have developed and used to simulate neutrino-induced air showers in the atmosphere. The main results of the paper are contained in §IV, where we show the outcome of our simulations and discuss the differences between ordinary air showers and BH-induced air showers. In §V, we briefly discuss possible detection techniques for BH formation based on  $\tau$  production in BH fragmentation. Finally, we conclude in §VI.

## II. BLACK HOLE PRODUCTION IN TEV GRAVITY

In models with  $n$  extra dimensions the fundamental coupling constant of gravity is the  $(n + 4)$ -dimensional Newton's constant

$$G_{n+4} \equiv M_{\star}^{-(n+2)}. \quad (1)$$

The observed four-dimensional Newton's constant  $G_4 \equiv M_{Pl}^{-2} = 6.707 \times 10^{-33} \text{ TeV}^{-2}$  and the  $(n + 4)$ -dimensional gravitational constant  $G_{n+4}$  are related by

$$G_4 = G_{n+4} V_n^{-1}, \quad (2)$$

where  $V_n$  is the volume of the extra dimensions. If  $V_n \gg M_{\star}^{-n}$ , it follows that  $M_{\star} \ll M_{Pl}$ . For the appropriate choices of  $n$  and  $V_n$ ,  $M_{\star}$  can be of the order of TeV energies such that gravity and the electroweak scales coincide. These models provide an attractive solution to the hierarchy problem of high-energy physics.

If gravity becomes strong at the electroweak scale, particle collisions with CM energy larger than a TeV can create BHs [12], branes [13, 14], and other nonperturbative gravitational objects [15, 16, 17]. BH formation dominates the gravitational channel if the extra-dimensional space is symmetric whereas branes form in asymmetric cases [13]. In this paper we only consider symmetric compactification and BH production since brane decay is even less understood than BH evaporation.

## A. Cross sections

The static and uncharged BH in  $(n+4)$ -dimensions is described by the  $(n+4)$ -dimensional Schwarzschild solution

$$ds^2 = -R(r)dt^2 + R(r)^{-1}dr^2 + r^2d\Omega_{n+2}^2, \quad (3)$$

where

$$R(r) = 1 - \left(\frac{r_s}{r}\right)^{n+1}. \quad (4)$$

The Schwarzschild radius  $r_s$  of the BH is related to the mass  $M_{BH}$  by

$$r_s = \frac{1}{\sqrt{\pi}M_\star} \left[ \frac{8\Gamma\left(\frac{n+3}{2}\right)}{(2+n)} \left(\frac{M_{BH}}{M_\star}\right) \right]^{\frac{1}{n+1}}. \quad (5)$$

At energy scales sufficiently above  $M_\star$ , BH formation is a semiclassical process. Thus the cross section can be approximated by an absorptive black disk with radius  $r_s$ . For a Schwarzschild BH the cross section is

$$\sigma_{ij \rightarrow BH}(s; n) = F(s)\pi r_s^2 = F(s) \frac{1}{s_\star} \left[ \frac{8\Gamma\left(\frac{n+3}{2}\right)}{(2+n)} \right]^{\frac{2}{n+1}} \left(\frac{s}{s_\star}\right)^{\frac{1}{n+1}}, \quad (6)$$

where  $\sqrt{s}$  is the CM energy of the collision,  $s_\star = M_\star^2$ , and  $F(s)$  is a form factor. Since  $M_{BH} \gtrsim M_\star$ , it follows that  $r_s \sim M_\star^{-1}$  and the cross section (6) must be interpreted at the parton level. The total cross section for a neutrino-proton event is obtained by summing over partons:

$$\sigma_{\nu p \rightarrow BH}(x_m; n) = \sum_{ij} \int_{x_m}^1 dx q_i(x, -Q^2) \sigma_{ij \rightarrow BH}(xs; n), \quad (7)$$

where  $q_i(x, -Q^2)$  are the parton distribution functions (PDFs) [42],  $-Q^2$  is the four-momentum transfer squared,  $x$  is the fraction of nucleon's momentum carried by the parton, and  $\sqrt{s x_m} = M_{BH, min}$  is the minimal BH mass for which the semiclassical cross section is valid (generally  $M_{BH, min} \sim \text{few } M_\star$ ).

Equation (7) should be interpreted with care as the total cross section value is affected by several sources of uncertainty. The first uncertainty comes from the approximate knowledge of the PDFs. For instance, the uncertainty in the gluon distribution (the most uncertain distribution) is  $\sim 15\%$  for  $x \lesssim 0.3$  and increases rapidly for large  $x$  [43]. Furthermore, the PDFs are known only for momentum transfer smaller than 10 TeV. In BH events we expect the

momentum transfer to be of the order of either the mass or the inverse Schwarzschild radius [44]. Therefore, the momentum transfer can reach hundreds of TeV in UHECR-induced BH events. In the calculation of the total cross section we fix the PDFs for momentum transfers above 10 TeV to be equal to the 10 TeV value. Although the dependence of the PDFs on the momentum transfer seems quite small (at least for momentum transfers smaller than 10 TeV), the 10 TeV cutoff on the momentum transfer induces an additional uncertainty in the integrated cross section Eq. (7). A conservative estimate of the total uncertainty due to the PDFs is  $\sim 20\%$ .

A second major source of uncertainty in Eq. (7) derives from the physics of BH formation at the parton level, which is presently not well understood. The theoretical uncertainties in the dynamics of the process at parton level are parametrized by the form factor  $F(s)$  and have been summarized in Refs. [18, 27]. The two main factors that may affect Eq. (6) are the uncertainty in the fraction of the initial CM energy that goes into the BH and the presence of angular momentum. Numerical simulations for head-on collisions in four dimensions suggest that the mass of the BH is smaller than the CM energy of the colliding particles, leading to a reduction of the total cross section. Rotating BHs have also smaller cross sections than non-rotating BHs. A naive estimate of the corrections due to angular momentum suggests a reduction of the cross section of about 40%. On the other hand, the non-relativistic limit of two-BH scattering indicates that the geometrical cross section can be enhanced by a factor  $\sim 250 - 350\%$ , depending on the spacetime dimension. The classical cross section for photon capture can also be used to obtain a crude estimate of the cross section of BH formation, suggesting an enhancement of the cross section by a factor ranging from 300% ( $n = 2$ ) to 87% ( $n = 7$ ).

To our knowledge, all the quantitative results of the past literature are obtained from Eq. (7) by setting  $F(s) = 1$  and neglecting the PDF uncertainties. (See, e.g., [26, 27, 28, 29].) This is partially motivated by the fact that an exact estimate of the total uncertainty in the BH cross sections due to the combined PDF and parton-level uncertainties is unattainable at present. However, the arguments listed above suggest that the cross section uncertainties range from  $\sim 40\%$  to  $\sim 300\%$  which can significantly affect most results. Throughout this paper, we take into account these uncertainties when deriving observables.

The cross section as a function of  $M_\star$ ,  $M_{BH,min}$ ,  $E_\nu$ , and the uncertainties described above are shown in Fig. 1. The upper left, upper right, and lower left panels show  $\sigma_{\nu p \rightarrow BH}$

as a function of  $M_{BH,min}$  for three different incoming neutrino energies ( $E_\nu = 10^6, 10^7,$  and  $10^8$  TeV), for different values of  $M_\star$  (disks for  $M_\star = 1$  TeV, triangles for  $M_\star = 2$  TeV, stars for  $M_\star = 5$  TeV, and circles for  $M_\star = 10$  TeV), and for the case of seven dimensions ( $n = 3$ , red symbols) and ten dimensions ( $n = 6$ , black symbols). The symbols give the cross section calculated from Eq. (7) setting  $F(s) = 1$  and neglecting the PDF uncertainties. The lower right panel shows the cross section as a function of energy for  $M_\star = 1$  TeV and ten dimensions. The red shaded (inner) region shows the uncertainty in the cross section due to the unknown  $M_{BH,min}$  which we vary from  $M_\star$  to  $10 M_\star$ . The green shaded (outer) region shows the uncertainty associated with the BH formation at the parton level and the PDF. The solid lines in the graphs show the cross section for SM interactions. The uncertainty in the SM cross section due to the unknown PDFs at very small values of  $x$  is bracketed by dashed lines.

For a given number of extra dimensions, the total cross section increases with the energy of the primary neutrino and decreases when the fundamental scale is increased. At fixed energy and  $M_\star$ , the cross section decreases with increasing  $M_{BH,min}$ . The overall effect makes the cross section at fixed energy vary by many orders of magnitude. For instance, the ten-dimensional total cross section at  $E_\nu = 10^8$  TeV spans five orders of magnitude, ranging from values of tens of pb to millions of pb, where the lower values are obtained for large fundamental scales. At fixed energy and  $M_\star$ , the range in cross section values span about an order of magnitude unless  $M_{BH,min}$  becomes comparable to the CM energy of the event. In this case, the rate of events is dramatically suppressed and the cross section tends to zero. The behavior of the total cross section with the energy at fixed  $M_\star$  is steeper for higher values of  $M_{BH,min}$ . In the range  $E_\nu = 10^6 - 10^9$  TeV, which is of interest to UHECRs, the cross section grows approximately like  $\sigma_{\nu p \rightarrow BH} \sim E_\nu^{0.4-1.8}$ , where lower exponents are obtained for lower  $M_{BH,min}$ . For example, in ten dimensions the behavior of the cross section is  $\sigma_{\nu p \rightarrow BH} \sim E_\nu^{0.41}$  for  $M_{BH,min} = M_\star = 1$  TeV,  $\sigma_{\nu p \rightarrow BH} \sim E_\nu^{0.67}$  for  $M_{BH,min} = 5 M_\star = 5$  TeV, and  $\sigma_{\nu p \rightarrow BH} \sim E_\nu^{0.77}$  for  $M_{BH,min} = 10 M_\star = 10$  TeV.

The large uncertainties in the values of  $\sigma_{\nu p \rightarrow BH}$  make it quite difficult to discriminate between different values of the fundamental scale  $M_\star$  with good precision. The range of possible  $\sigma_{\nu p \rightarrow BH}$  for a given  $M_\star$  overlaps with the range for larger  $M_\star$  because of the theoretical uncertainties. Even if  $\sigma_{\nu p \rightarrow BH}$  were to be constrained by experiments,  $M_\star$  could not be determined unless the degeneracy were removed by additional assumptions on  $M_{BH,min}$  and

by reducing other theoretical uncertainties in  $\sigma_{\nu p \rightarrow BH}$ . The dependence of the cross section on  $n$  is the least dramatic making it also hard to differentiate between different dimensions. In addition, as  $M_\star$  becomes larger than  $\sim 1$  TeV,  $\sigma_{\nu p \rightarrow BH}$  becomes smaller than the cross section for SM interactions and the probability for BH formation decreases accordingly.

## B. BH evaporation products

Once the CM energy of a neutrino collision with a nucleon in the air reaches the BH formation threshold, a BH with initial mass equal to a fraction of the total CM energy may form. The distribution of the initial BH masses is given by the differential cross section

$$\frac{d\sigma_{\nu p \rightarrow BH}}{dM_{BH}} = 2 \left(\frac{x}{s}\right)^{1/2} q_i(x, -Q^2) \sigma_{ij \rightarrow BH}(xs; n). \quad (8)$$

Light BHs are favored over heavy BHs. The typical initial BH mass is usually a few times  $M_{BH,min}$ . Therefore, models with larger (smaller) fundamental Planck scale tend to produce higher (lower) mass BHs. The integrated probability of BH formation vs the initial BH mass is plotted in Fig. 2 for a neutrino energy  $E_\nu = 10^7$  TeV,  $n = 6$ ,  $M_\star = 5$  TeV and  $M_{BH,min} = 1, 3, 5, 10 M_\star$ . The initial BH mass is very sensitive to the value of  $M_{BH,min}$ . For  $M_{BH,min} = M_\star$ , 90% of the formed BHs have initial mass less  $\sim 20$  TeV, whereas for  $M_{BH,min} = 10 M_\star$  the 90% threshold is reached at  $M_{BH} \sim 80$  TeV.

Once formed, the BH decay phase is expected to proceed in three stages: classical, semiclassical, and quantum [22]. In the first stage the BH sheds the hair associated with gauge charges and angular momentum. In the second stage the BH evaporates semiclassically by emission of thermal Hawking radiation with temperature  $T_H$ . We assume that most of the energy is radiated into the brane, as only gravitons can “see” the bulk [45, 46]. The Hawking evaporation ends when the mass of the BH approaches  $\sim M_\star$ . At this point the semiclassical description breaks down and the BH may either decay completely by emitting a few quanta with energy of order of  $M_\star$  or leave a stable remnant with mass  $\sim M_\star$  [47]. The details of this last stage depends on the unknown underlying quantum theory. However, the semiclassical decay should lead to most of the observable signatures. During the semiclassical evaporation, the BH decays in a time (CM frame) [46]

$$\tau \sim \frac{1}{M_\star} \left(\frac{M_{BH}}{M_\star}\right)^{\frac{n+3}{n+1}}. \quad (9)$$

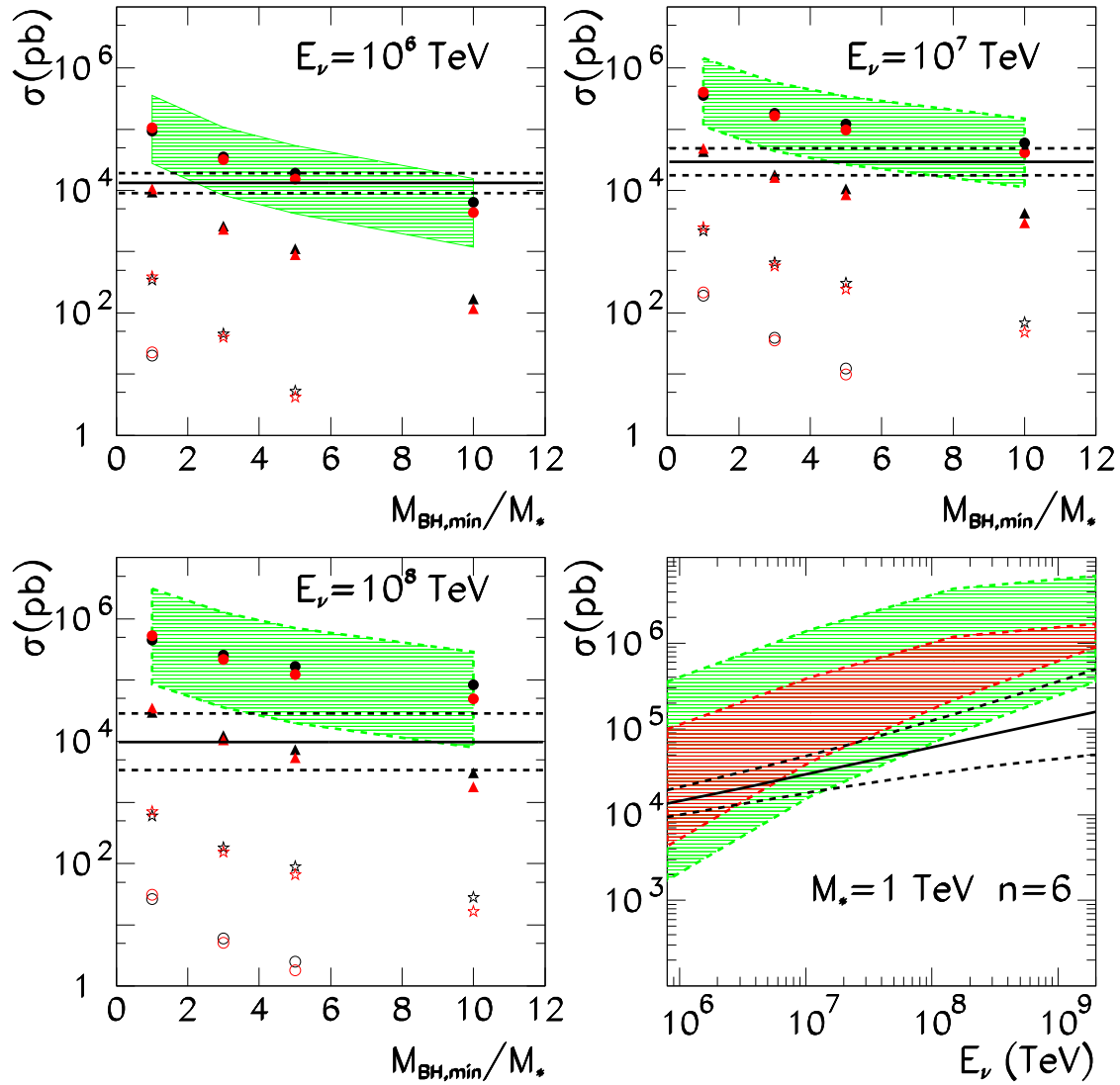


FIG. 1: The two upper panels and the lower left panel show  $\sigma_{\nu p \rightarrow BH}(M_{BH,min}/M_*)$  for  $E_\nu = 10^6, 10^7, \text{ and } 10^8$  TeV. The disks, triangles, stars, and circles are for  $M_* = 1, 2, 5, \text{ and } 10$  TeV, respectively. The red (black) symbols are for  $n = 3$  ( $n = 6$ ). The shaded regions show the uncertainties. The lower right panel shows  $\sigma_{\nu p \rightarrow BH}(E_\nu)$  for  $n = 6$  and  $M_* = 1$  TeV, with the  $M_{BH,min}$  range in red (inner shaded region) and the uncertainties at the parton level and PDF in green (outer shaded region). The solid lines give the SM cross section, with dashed lines showing PDF uncertainties.

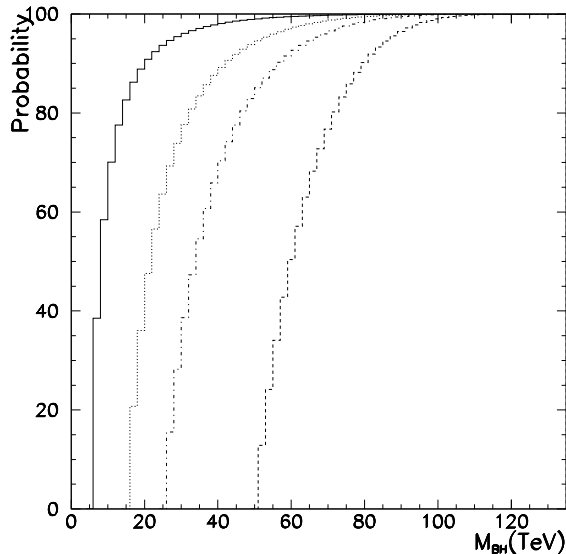


FIG. 2: Integrated probability of BH formation as a function of the initial BH mass for  $E_\nu = 10^7$  TeV,  $n = 6$ ,  $M_\star = 5$  TeV, and  $M_{BH,min} = 1$  (solid line), 3 (dotted line), 5 (dashed line), and 10 (long-dashed line)  $M_\star$ .

Assuming a Boltzmann statistics and instantaneous BH evaporation, the BH emits an average number of quanta [23]

$$\langle N \rangle = \frac{M_{BH}}{2T_H}, \quad (10)$$

where the Hawking temperature  $T_H$  is related to the Schwarzschild radius and to the entropy of the BH,  $S_{BH}$ , by [48]

$$T_H = \frac{n+1}{4\pi r_s} = \frac{n+1}{n+2} \frac{M_{BH}}{S_{BH}}. \quad (11)$$

In Table I, we list the parameters of typical BHs in ten and six dimensions for different choices of  $M_\star$  and of the BH mass ( $M_{BH} = 5, 10, 50,$  and  $100$  TeV). The particle emission rate for a BH with temperature  $T_H$  is given by [49, 50]

$$\frac{dN_i}{dE dt} = \frac{c_i \Gamma_{s_i} A_c}{8\pi^2} \frac{E^2}{e^{E/T} - (-1)^{2s_i}}, \quad (12)$$

where  $E$  is the energy,  $A_c$  is the optical area of the BH [45], and  $\Gamma_i$ ,  $c_i$ ,  $\sigma_{s_i}$ , and  $N_i$  are the spin, the degrees of freedom, the greybody factors, and the number of quanta of the particle of species  $i$ . We neglect particle masses which are generally much smaller than the BH mass.

TABLE I: Decay time in the CM frame ( $\tau$ , in units of  $10^{-26}$  s), initial temperature ( $T_H$  in TeV), initial entropy ( $S$ ), average number of produced quanta ( $\langle N \rangle$ ), and energy per quantum ( $E/\langle N \rangle$  in TeV) of Schwarzschild BHs for various  $M_\star$  (TeV),  $M_{BH}$  (TeV),  $n = 6$  and  $n = 3$  (in parentheses).

$M_\star$	$M_{BH}$	$\tau$	$T_H$	$S$	$\langle N \rangle$	$E/\langle N \rangle$
1	5	0.521 (0.736)	0.553 (0.282)	8 (14)	5 (9)	1.11 (0.56)
1	10	1.27 (2.08)	0.500 (0.237)	17 (34)	10 (21)	1.00 (0.47)
1	50	10.1 (23.3)	0.398 (0.159)	110 (252)	63 (158)	0.80 (0.32)
1	100	24.5 (65.8)	0.360 (0.133)	243 (600)	139 (375)	0.72 (0.27)
2	5	0.107 (0.130)	1.22 (0.671)	4 (6)	2 (4)	2.44 (1.34)
2	10	0.261 (0.368)	1.11 (0.564)	8 (14)	5 (9)	2.21 (1.13)
2	50	2.06 (4.11)	0.878 (0.377)	50 (106)	28 (66)	1.76 (0.76)
2	100	5.03 (11.6)	0.795 (0.317)	110 (252)	63 (158)	1.59 (0.64)
5	5	0.013 (0.013)	3.48 (2.11)	1 (2)	1 (1)	6.95 (4.22)
5	10	0.032 (0.037)	3.15 (1.77)	3 (5)	2 (3)	6.30 (3.55)
5	50	0.254 (0.416)	2.50 (1.19)	17 (34)	10 (21)	5.01 (2.37)
5	100	0.620 (1.18)	2.27 (0.997)	39 (80)	22 (50)	4.53 (2.00)
10	10	0.007 (0.007)	6.95 (4.22)	1 (2)	1 (1)	13.9 (8.44)
10	50	0.052 (0.074)	5.53 (2.82)	8 (14)	5 (9)	11.1 (5.64)
10	100	0.127 (0.208)	5.01 (2.37)	17 (34)	10 (21)	10.0 (4.74)

Integrating Eq. (12) over  $E$  gives

$$\frac{dN_i}{dt} = c_i \Gamma_{s_i} f_i \frac{AT^3}{8\pi^2} \Gamma(3) \zeta(3) = c_i \Gamma_{s_i} f_i \frac{\zeta(3) T (n+3)^{\frac{n+3}{n+1}} (n+1)}{16\pi^3 2^{\frac{2}{n+1}}}, \quad (13)$$

where  $f_i = 1$  (3/4) for bosons (fermions). Since the observed Hawking emission happens on the brane, we use the four-dimensional greybody factors of Ref. [51]. (Greybody factors in  $n + 4$  dimensions have been calculated in Refs. [52, 53, 54]. See also Ref. [55, 56] for a discussion on BH recoil effect.) The values of  $s_i$ ,  $c_i$ ,  $\Gamma_{s_i}$ , and  $f_i$  are listed in Table II.

The number ratio of two particle species  $i$  and  $j$  is [46]:

$$\frac{N_i}{N_j} = \frac{c_i \Gamma_{s_i} f_i}{c_j \Gamma_{s_j} f_j}. \quad (14)$$

Using Eq. (10),  $N_i$  can be expressed as

$$N_i = \langle N \rangle \frac{c_i \Gamma_{s_i} f_i}{\sum_j c_j \Gamma_{s_j} f_j}. \quad (15)$$

The number of each particle species formed for the BHs listed in Table I for  $M_\star = 1$  TeV is given in Table III.

TABLE II: The values of  $s_i$ ,  $c_i$ ,  $\Gamma_{s_i}$ ,  $f_i$  for the SM particles

species	$s_i$	$c_i$	$\Gamma_{s_i}$	$f_i$
quark	1/2	72	0.6685	3/4
charged lepton	1/2	12	0.6685	3/4
neutrino	1/2	6	0.6685	3/4
Higgs	0	1	1	1
photon	1	2	0.2404	1
gluon	1	24	0.2404	1
$W$	1	6	0.2404	1
$Z$	1	3	0.2404	1
graviton	2	2	0.0275	1

For example, a BH of mass  $M_{BH} = 50$  TeV and  $M_\star = 1$  TeV according to Table I emits 63 quanta, each with energy of 0.80 TeV. These quanta are translated into SM particles some of which decay or hadronize. The final output of the BH evaporation may contain up to  $\sim 2000$  particles.

### III. EXTENSIVE AIR SHOWER SIMULATIONS

Extensive air showers created by ultrahigh energy interactions in the atmosphere can be detected with ground arrays and fluorescence telescopes. Ground arrays record the signal which is produced by the particles of the shower reaching the ground. Fluorescence telescopes observe the fluorescence light produced by the interaction of the atmospheric nitrogen molecules with the electromagnetic component of the developing air shower. The fluorescence method pioneered by the Fly's Eye [57, 58] detector is able to reconstruct the

TABLE III: Fragmented number of particle species for  $n = 6$  ( $n = 3$ ),  $M_\star = 1$  TeV

$M_{BH}$ (TeV)	5	10	50	100
quark	3 (6)	7 (14)	42 (104)	92 (248)
c. lepton	0 (1)	1 (2)	7 (17)	15 (41)
neutrino	0 (0)	1 (1)	3 (9)	8 (21)
Higgs	0 (0)	0 (0)	1 (3)	3 (7)
photon	0 (0)	0 (0)	1 (1)	1 (3)
gluon	0 (1)	1 (2)	7 (17)	15 (40)
$W$	0 (0)	0 (1)	2 (4)	4 (10)
$Z$	0 (0)	0 (0)	1 (2)	2 (5)
graviton	0 (0)	0 (0)	0 (0)	0 (0)

longitudinal development of the  $e^+e^-$  component of the air shower. Fluorescence detectors are currently used by the HiRes [59] and Auger [60] experiments and are planned for the future EUSO [61] and OWL [62] observatories. This technique provides a good estimate of the energy of the primary particle that initiate the air shower, since most of the energy of the air shower goes into the observable electromagnetic channel. Another advantage of the fluorescence technique is the ability to reconstruct the depth at which the cascade contains the maximum number of  $e^+e^-$  pairs, i.e., the depth of shower maximum,  $X_m$ . This parameter is sensitive to the type of primary particle, to its energy and to the interaction initiating the cascade. The depth of the first interaction point,  $X_0$ , depends on the total cross section of the particle considered. Due to the small values of the neutrino-air cross sections, ultrahigh energy neutrinos can induce air showers at any depth in the atmosphere such that  $X_0$  is arbitrary.

Neutrinos can interact at any depth in the atmosphere with almost equal probability. The interaction length of a neutrino with energy  $E_\nu = 10^9$  TeV is  $\lambda_{\nu CC} \simeq 1.1 \times 10^7$  g cm $^{-2}$  for the charged current (CC) interactions. This is larger than the column depth of the atmosphere in the horizontal direction, which is  $3.6 \times 10^4$  g cm $^{-2}$ . BH forming interactions do not improve this situation as the BH formation cross sections cannot be not much greater than the SM values (see Fig. 1). For example, if  $M_\star = 1$  TeV and  $n = 6$ ,  $\lambda_{\nu BH} \simeq 1.7 \times 10^5$  g cm $^{-2}$ . Fig. 3

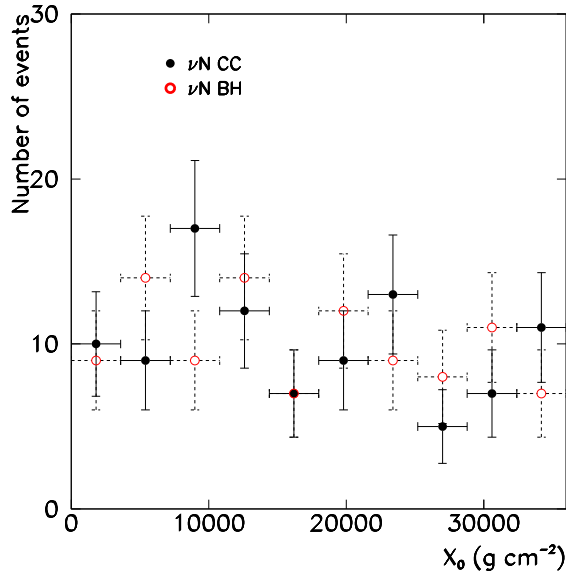


FIG. 3: The  $X_0$  distribution for 100 neutrinos with  $E_\nu = 10^9$  TeV interacting in a column depth of  $3.6 \times 10^4$  g cm $^{-2}$ . The SM CC interaction length is  $\lambda_{\nu CC} \simeq 1.1 \times 10^7$  g cm $^{-2}$  (solid error bars). The BH interaction length is  $\lambda_{\nu BH} \simeq 1.7 \times 10^5$  g cm $^{-2}$  for  $M_\star = 1$  TeV and  $n = 6$  (dashed error bars).

shows that the  $X_0$  distribution is flat for SM and BH interactions. Thus the  $X_m$  distribution is also flat. As we discuss below, differences between SM and BH interactions are evident in  $X_m - X_0$ . We can directly compare the values of  $X_m$  by fixing the value of  $X_0$  in the simulations.

We developed a Monte Carlo code to study the air showers induced by BH formation in neutrino-air collisions and compare the BH-induced air showers to the SM neutrino-induced air showers. The code generates observable secondaries from SM neutrino interactions and BH evaporation using the PYTHIA (ver. 6.2) package [40]. These secondaries are then injected into the AIRES simulator as primaries for the final air shower. In the AIRES code the threshold energy for tracking particles in the air showers are 80 keV for gamma rays, 80 keV for electrons and positrons, 1 MeV for muons, 500 keV for mesons and 150 MeV for nucleons. The geomagnetic field is set to the Pierre Auger Observatory. The “thinning” level used in this work is  $10^{-5}$  with a weight limitation of 20. (Thinning is a method commonly used in simulations of UHECRs to avoid following the huge number of secondary particles

by following only a fraction of them with varying weights. See [41] for further details.)

### A. SM neutrino-induced air showers

We simulate the air showers induced by CC and neutral current (NC) interactions by the following procedure:

- The differential cross sections are integrated over the fraction of the total momentum of the nucleon carried by the parton ( $x$ ) for all the possible values of the fraction of total energy that goes into the hadronic cascade ( $y$ ).
- A value of  $y$  is sampled from the previous distribution. The mean value of  $y$  at the energies relevant for UHECRs is 0.2.
- The energy of the lepton (CC interaction) or neutrino (NC interaction) in the final state is given by  $(1-y) E_\nu$ . The CC lepton is injected into AIRES.  $\tau$  leptons cannot be simulated by AIRES. Therefore, we calculate the decay length and use the PYTHIA generator to obtain the secondaries, which are then injected at the corresponding height at which the  $\tau$  decays. Note, however, that the  $\tau$  particles have a mean energy of  $0.2E_\nu$ , so most  $\tau$ 's reach the ground without decaying and are not converted into observable energy. The NC neutrino is not observable and is not injected in AIRES.
- The hadronic part of the CC and NC interactions are simulated with PYTHIA. The secondary particles are then injected in AIRES.

### B. BH-induced air showers

A similar Monte Carlo code is used to simulate air showers induced by BH formation. The BH simulation follows this procedure:

- The mass of BH is calculated using the probabilities given by Eq. (8). The gamma factor of the BH is  $\gamma = E_\nu/M_{BH}$ . Different cases of  $M_{BH,min}$  are considered.
- The temperature of the BH, and the energy and total number of quanta emitted in the evaporation phase are calculated for different choices of  $n$  and  $M_\star$ . The fragmented number of particles species is computed (as in Table III).

- The momentum of each quanta in the rest frame of the BH are calculated assuming an isotropic distribution. If the quantum generated is a quark or a gluon, the secondaries resulting from the parton cascade of this quantum are calculated using PYTHIA. If the quantum is a gauge boson, it is decayed using PYTHIA. The momenta of all the particles are then boosted to the laboratory system.
- The secondaries are injected in the AIRES code to simulate the extensive air shower. All the secondaries are injected at the assumed first interaction point except for the  $\tau$  particles which are dealt with as in the SM air showers. However, the energy of the  $\tau$  particles generated by BH evaporation is generally smaller than the energy of the  $\tau$ 's generated in the SM process. The decay length of BH  $\tau$ 's is comparatively shorter than in the SM case. Neutrinos, gravitons, and  $\tau$ 's that decay after reaching the ground are not observable, thus they are not injected in AIRES.
- $\pi^0$ 's generated by the hadronization of quarks, gluons, and gauge bosons are immediately decayed by PYTHIA. This is a good approximation since the average pion energy is smaller than the critical energy. Therefore,  $\pi^0$ 's are more likely to decay than interact.

## IV. SIMULATION RESULTS

### A. Neutrino-initiated air showers

We simulated SM-induced air showers for CC and NC interactions as well as air showers from BH production. The showers were chosen to have a zenith angle of  $70^\circ$  and a primary neutrino energy  $E_\nu = 10^7$  TeV. The first interaction point was fixed to an altitude of 10 km corresponding to a slant depth of  $780 \text{ g cm}^{-2}$ .

SM neutrino air showers are generally dominated by CC interactions because NC interactions have lower cross section,  $\sigma_\nu^{NC} = 0.4 \sigma_\nu^{CC}$ . Moreover, a large fraction of the primary neutrino energy of the NC interaction,  $(1 - y) E_\nu \sim 0.8 E_\nu$ , is carried out by the scattered neutrino and is not observable. Similarly, the CC  $\nu_\mu$  scattering produces a high energy invisible  $\mu$  that does not contribute to the shower energy. The CC  $\nu_\tau$  interaction produces a high energy  $\tau$  that generally does not decay before reaching ground level. For  $E_\nu = 10^7$  TeV,

the decay length of the scattered  $\tau$  is  $\sim 500$  km. If the  $\tau$ 's were to decay before reaching the ground, the air shower would appear as a superposition of showers initiated at different heights. (We will return to  $\tau$  decay later in §V.) Therefore, as far as CC interactions are concerned, the most easily observed primary is the  $\nu_e$ . The secondary electron initiates a purely electromagnetic air shower that carries  $\sim 80\%$  of the primary neutrino energy. These showers have similar features to electromagnetic air showers:

- CC  $\nu_e$  air showers are  $\mu$ -poor. The dominant process for  $\mu$  production in an electromagnetic cascade is photoproduction. The ratio of the pair production and photoproduction cross sections determines the number of  $\mu$ 's in the air shower. This ratio is  $2.8 \times 10^{-3}$  at  $10^{-2}$  GeV and is expected to be  $\sim 10^{-2}$  at  $\sim 10^7$  TeV.
- CC  $\nu_e$  air showers develop slower than hadronic air showers. The number of secondaries in pair production or bremsstrahlung interactions is smaller than in hadronic interactions. Additionally, the Landau-Pomeranchuk-Migdal (LPM) effect [63, 64, 65, 66] also contributes in slowing down the shower development once primary energies reach above  $E_{LPM} \sim 10^7$  TeV [67, 68].

We performed a systematic simulation of SM neutrino-induced air showers and checked the characteristics discussed above. Here, we only show the more relevant CC-induced air showers and compare them to the BH-induced air showers. The left panel in Fig. 4 shows the longitudinal development of CC- and BH-induced air showers. We chose the BH parameters  $M_{BH,min} = 2 M_\star = 2$  TeV and  $n = 6$ . A difference of  $\sim 200$  g cm $^{-2}$  in  $X_m$  is evident between the SM and BH events. This large difference results from the combination of the large multiplicity and hadronic nature of BH-induced air showers and electromagnetic nature of the CC-induced air showers.

BH-induced air showers generally develop faster than typical SM hadronic air showers depending on the initial and minimum masses of the BH that give the number of produced quanta. For example, if  $M_{BH,min} = 2 M_\star = 2$  TeV and  $n = 6$ , the average BH mass is  $\langle M_{BH} \rangle \sim 7$  TeV which produces about seven quanta. If all the quanta are quarks, gluons or gauge bosons, the number of secondaries produced is  $\sim 200$ . This number of secondaries is also close to the mean multiplicity for a SM proton-N $^{14}$  collision with energy  $10^7$  TeV in the laboratory frame. However, in SM hadronic interactions most of the momentum is carried by the leading baryon, the other 199 particles are softer. In the BH case, the momentum is

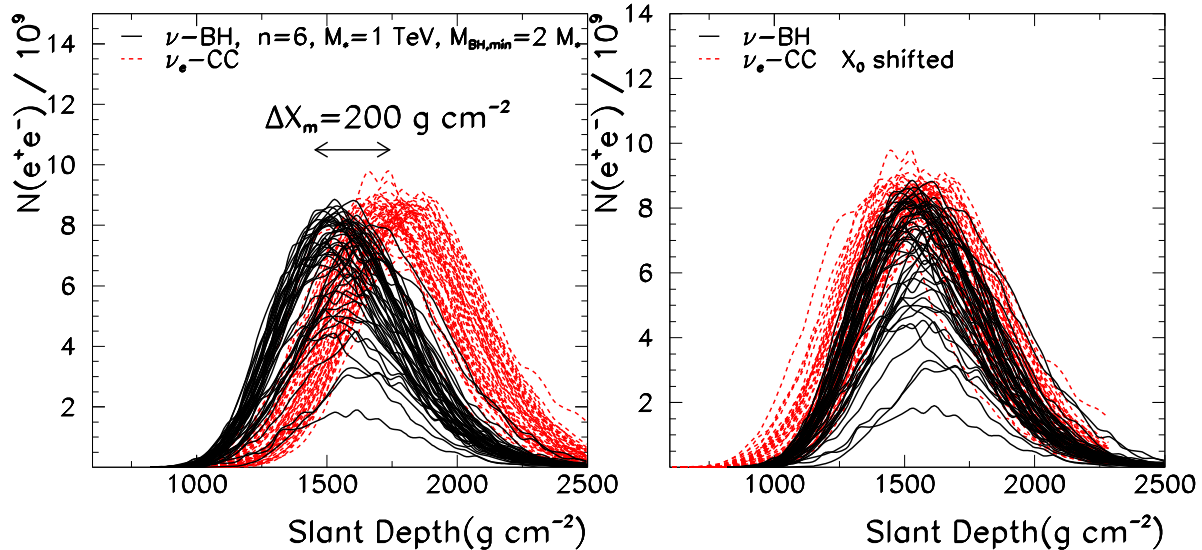


FIG. 4: Number of  $e^+e^-$  vs slant depth for neutrino air showers with  $E_\nu = 10^7$  TeV. The SM CC air showers are shown in red (dashed lines) and the BH-induced air showers with  $n = 6$  and  $M_{BH,min} = 2M_\star = 2$  TeV are shown in black (solid lines). The left panel has fixed  $X_0(CC) = X_0(BH)$ . The right panel has shifted  $X_0$  such that  $X_m(CC) \simeq X_m(BH)$ .

equally shared by all the quanta such that the shower produces 200 similar secondaries in the first interaction which causes a faster shower development.

If the first interaction point could be observed, the difference between the BH and the SM value of  $X_m - X_0$  would be clearly distinguished on an event-by-event basis (see Fig. 4 left panel). However,  $X_0$  cannot be directly observed due to limited sensitivity of the detectors. The right panel in Fig. 4 shows the events with the SM curves shifted by  $200 \text{ g cm}^{-2}$  and renormalized. The difference between the two cases is no longer apparent.

CC-induced air showers have large fluctuations in  $X_m - X_0$  (Fig. 4). This is mainly due to fluctuations in the fraction of primary energy carried by the scattered electron. This fraction is usually large such that CC-induced air showers behave often like electromagnetic air showers. On the odd occasion that a large fraction of the primary energy is carried by partons, the air shower is closer to a hadronic air shower. In addition, the LPM effect increases the fluctuations in  $X_m - X_0$  of electromagnetic air showers, if the energy of the scattered electron ( $yE_\nu$ ) is larger than  $E_{LPM}$ . On the other hand, the number of particles

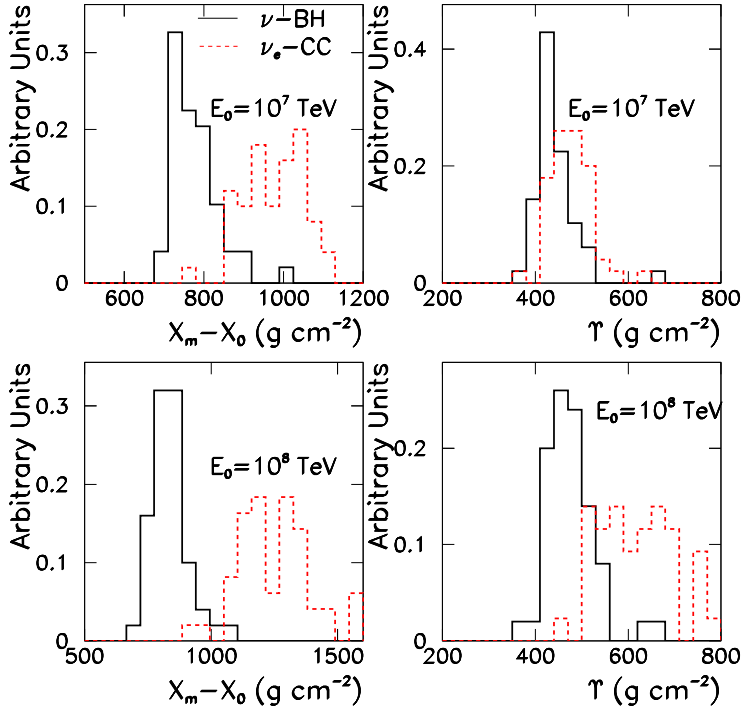


FIG. 5: The left panels show the  $X_m - X_0$  distribution for SM and BH air showers with  $n = 6$  and  $M_{BH,min} = 2 M_* = 2$  TeV. The right panels show the distribution of the rise-depth parameter,  $\Upsilon$ , for the same showers. The upper (lower) panels correspond to  $E_\nu = 10^7$  ( $10^8$ ) TeV.

at shower maximum,  $N_{max}$ , is proportional to the primary particle energy, which is more stable in the electromagnetic cascade case (fluctuations in  $N_{max}$  are on the  $\sim 5\%$  level).

In contrast, BH-induced air showers have small fluctuations in  $X_m - X_0$  and large fluctuations in  $N_{max}$ . The fluctuations in  $X_m - X_0$  are consistent with the fluctuations of SM hadronic-induced air showers. The large fluctuation in  $N_{max}$  ( $\sim 20\%$ ) is due to the superposition of two effects: (i) Each quantum usually carries a large fraction of the primary energy and (ii) some of the produced quanta do not contribute to the shower energy (neutrinos, gravitons,  $\mu$ 's, and non-decaying  $\tau$ 's).

The left panels of Fig. 5 show the  $X_m - X_0$  distribution for neutrino SM and BH air showers. For  $E_\nu = 10^7$  ( $10^8$ ) TeV, the average  $X_m - X_0$  for BH-induced air showers is 770 (840)  $\text{g cm}^{-2}$  and 970 (1250)  $\text{g cm}^{-2}$  for SM-induced air showers. The spread is 62 (72)  $\text{g cm}^{-2}$  and 75 (140)  $\text{g cm}^{-2}$ . The difference between the BH and CC air showers increases

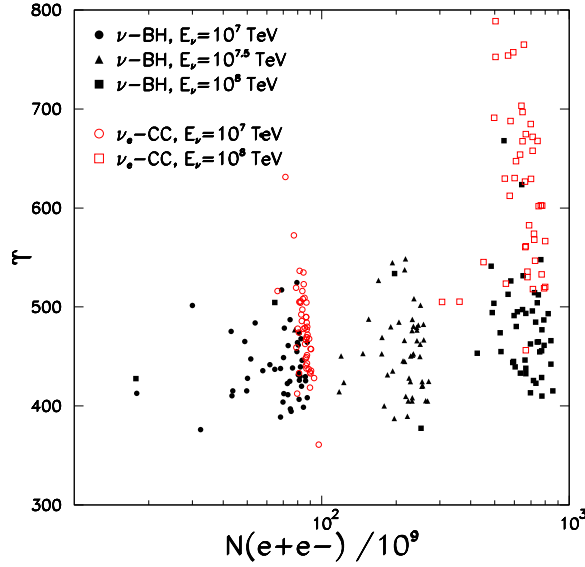


FIG. 6: Scatter plot of  $\Upsilon$  vs  $N_{max}$  for CC air showers (red void symbols) and BH air showers (black filled symbols) with  $n = 6$  and  $M_{BH,min} = 2 M_* = 2$  TeV. The disks are for  $E_\nu = 10^7$ , the circles for  $E_\nu = 10^8$  TeV, and the triangles for  $E_\nu = 10^{7.5}$ .

with the energy because the difference between hadronic and electromagnetic air showers also increases with energy (below  $E_\nu = 10^7$  TeV BH and SM showers are indistinguishable). Since  $X_0$  is not observable, we define an observable “rise-depth” parameter for each individual shower,  $\Upsilon \equiv X_m - X_{0.1}$ , where  $X_{0.1}$  is the slant depth where the shower has 10 % of particle content of the shower maximum.  $\Upsilon$  is a more realistic parameter as a discriminator between BH- and CC-initiated air showers because it is observable. The right panels of Fig. 5 show the  $\Upsilon$  distributions for SM- and BH-induced air showers at energies  $E_\nu = 10^7$  TeV (upper panel) and  $10^8$  TeV (lower panel). The separation between the distributions is evident at  $E_\nu = 10^8$  TeV. This trend is better seen in Fig. 6 where  $\Upsilon$  vs  $N_{max}$  is plotted for different primary energies. To clearly see the difference in the distributions it would be necessary to accumulate a large number of neutrino air showers. For the cosmogenic neutrino flux, we would expect one  $10^8$  TeV neutrino for every dozen  $10^7$  TeV neutrinos [38]. However, the cosmogenic neutrino flux is barely detectable by experiments under construction; at most a few events between  $10^6$  and  $10^7$  TeV are expected to be detected per year [69, 70, 71]. Either there are larger unexpected fluxes of neutrinos or larger detectors will be needed that

can accumulate enough statistics to discriminate between BH and SM interactions through the  $\Upsilon$  distribution.

We also simulated the longitudinal development of  $\mu$ 's for each individual shower. Since  $\mu$ 's are detected on the ground, we calculated the  $\mu$  number for different positions of the ground detector relative to  $X_m$ . In Fig. 7, we show the number of  $\mu$ 's vs  $N_{max}$  for 50 air showers at a depth  $X_m + \Delta X$ , where  $\Delta X = 168, 336, \text{ and } 672 \text{ g cm}^{-2}$ .  $N_{max}$  is essentially proportional to the observed energy. CC-induced air showers are  $\mu$ -poor because of their electromagnetic nature, whereas BH-induced air showers are  $\mu$ -rich like hadronic air showers.

To summarize, two features should be used to find evidence of BH formation in extensive air showers: the rise depth and the  $\mu$  content of the air showers. The main differences arise from the electromagnetic nature of the CC-induced air showers in contrast to the hadronic character of the BH air showers. To take advantage of the differences in  $\mu$  content and the  $\Upsilon$  distribution, an experiment should combine both ground and fluorescence observations for each individual air shower. The Pierre Auger Observatory is the first such hybrid detector consisting of a ground array which sample the particle content at a given depth, looked over by four fluorescence detectors which may determine  $X_m$  and  $\Upsilon$ . For shower core distances larger than  $\sim 1 \text{ km}$  and  $\Delta X$  larger than  $\sim 100 \text{ g cm}^{-2}$  most of the signal recorded in the ground detectors is dominated by  $\mu$ 's and thus is directly sensitive to the difference in  $\mu$  content between BH and CC-induced air showers. The only challenge for the Auger observatory to test the BH hypothesis is the low neutrino flux. If the ultrahigh energy neutrino flux is at the level of the expected cosmogenic flux, a larger version of the Auger hybrid detector would be needed to test these theories.

## B. Shower dependence on BH parameters

In the previous sections we compared SM- and BH-induced air showers for  $n = 6$  and  $M_{BH,min} = 2M_\star = 2 \text{ TeV}$ . The previous results can be generalized to different choices of these parameters. The two quantities that characterize the BH air showers are the cross section and the multiplicity of particles. The cross section uncertainties considered in §II affect the first interaction point, but do not affect the shower development. The main factors that can change the physical characteristics of the air showers are the multiplicity and the nature of secondaries originated from the BH evaporation.

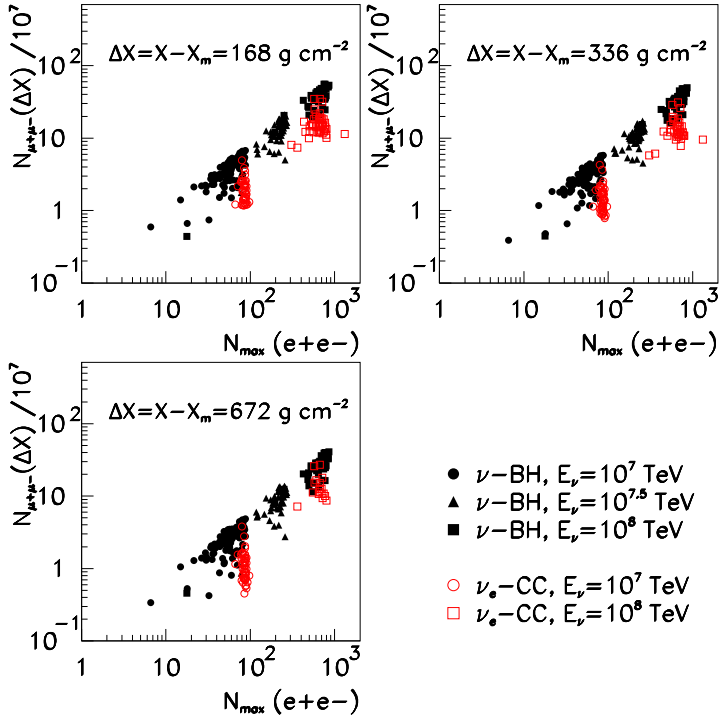


FIG. 7:  $\mu$  number distribution at a depth  $X_m + \Delta X$  vs  $N_{max}$  for 50 simulated air showers with  $E_\nu = 10^7, 10^{7.5}, 10^8$  TeV. The red void (black filled) symbols correspond to SM-induced (BH-induced) air showers ( $n = 6$  and  $M_{BH,min} = 2M_\star = 2$  TeV).  $N_{max}$  gives the observed energy of the event.

The multiplicity is controlled by the mean number of quanta,  $N_q$ , produced in the BH evaporation. Most of these quanta are quarks and gluons that hadronize and initiate a number of hadronic cascades with average energy (laboratory frame)  $E_q = \gamma M_{BH}/N_q$ . These sub-showers reach a maximum at the same depth. Thus the maximum of the shower, which is the sum of all sub-showers, is given by the maximum of a hadronic air shower with energy  $E_q$ . The shower maximum has a logarithmic dependence on the energy:

$$X_m = X_0 + A \log_{10} \left[ \frac{E_\nu}{N_q \text{ TeV}} \right] + B. \quad (16)$$

The simulations give  $A \sim 60\ g\ cm^{-2}$  and  $B \sim 311\ g\ cm^{-2}$ .  $A$  is the change in  $X_m - X_0$  per decade of energy and is analogous to the more commonly used elongation rate, which is the change in  $X_m$  per decade of energy. Our results agree well with the experimental results and previous simulations that give an elongation rate  $\sim 60\ g\ cm^{-2}$  [72].

The number of quanta depends on the BH mass and differs for each individual air shower. Moreover, the number of quanta varies with  $M_\star$  and  $n$  at fixed energy. The shift in the shower maximum of two distinct showers initiated by  $N_{q1}$  and  $N_{q2}$  quanta is

$$X_{m1} - X_{m2} = A \log_{10} \frac{N_{q2}}{N_{q1}} . \quad (17)$$

For instance, if the number of quanta increases by a factor of 3 (10),  $X_m$  decreases by 29 (60) g cm<sup>-2</sup>.

The left panel of Fig. 8 compares the longitudinal development of BH-induced air showers for  $n = 3$  and  $n = 6$ , with  $M_{BH,min} = 2M_\star = 2$  TeV. The primary energy is set to  $E_\nu = 10^7$  TeV, and  $X_0$  is the same for both air showers. The number of quanta produced in the BH evaporation decreases for larger  $n$ . Approximately three times more quanta are produced for  $n = 3$  at fixed  $M_{BH}$ . This translates into a shift in  $X_m$  of  $\sim 25$  g cm<sup>-2</sup>.

The right panel of Fig. 8 shows  $X_m$  for  $M_\star = 1$  TeV and 5 TeV with  $n = 6$  and  $M_{BH,min} = 2M_\star$ . At fixed  $M_{BH}$  the number of quanta for  $M_\star = 1$  TeV is six times larger than for  $M_\star = 5$  TeV. However, as  $M_{BH}$  is usually slightly larger than  $M_{BH,min}$ , the  $M_\star = 5$  TeV case starts with a more massive BH overall and hence produces a larger number of quanta than  $M_\star = 1$  TeV case (see Fig. 2). These two effects counteract and compensate each other, leading to the same number of quanta for both cases and no shift in  $X_m$  as shown in Fig. 8.

Fig. 9 shows the variation in the longitudinal development for  $M_{BH,min} = 2M_\star$  and  $10M_\star$ .  $M_{BH}$  changes by a factor five, thus increasing the number of quanta by the same factor. This is translated into a shift in  $X_m$  of  $\sim 50$  g cm<sup>-2</sup>, in good agreement with Eq. (17).

The variation of  $X_m$  with  $M_\star$  and the number of dimensions have no effect on the conclusions obtained in the previous section. The two parameters discussed to discriminate between BH- and SM-induced air showers do not depend on the position of the shower maximum. The observable signatures are based on the difference between the electromagnetic nature of the CC-induced air showers and the hadronic nature of the BH-induced air showers. Therefore, deeply penetrating horizontal hadronic-looking air showers will generally signal BH formation.

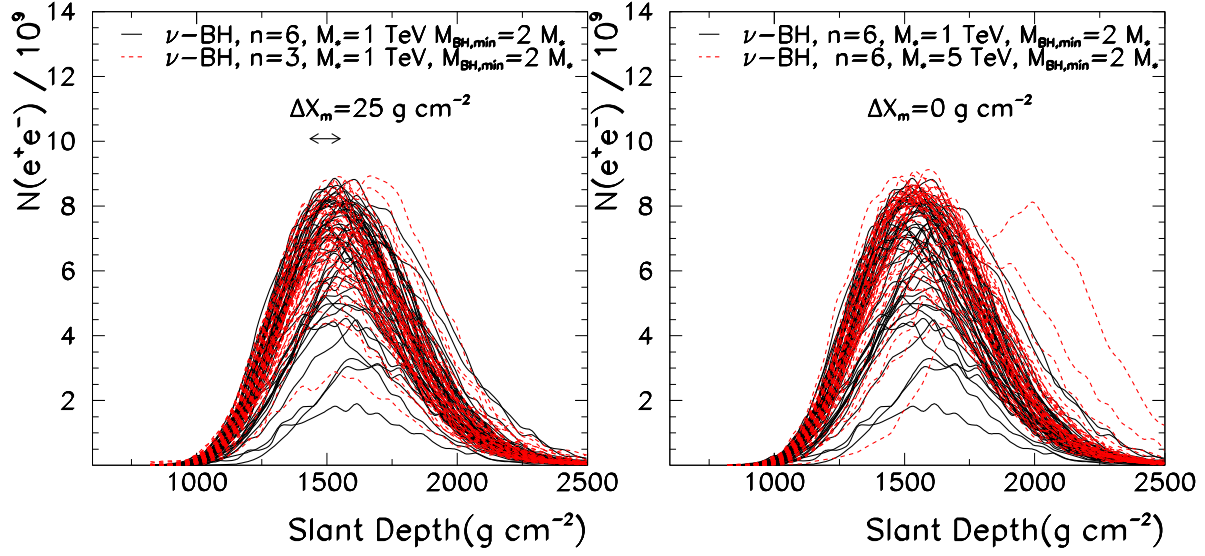


FIG. 8: Number of  $e^+e^-$  vs slant depth for BH-induced air showers. The left panel shows  $n = 6$  (black solid lines) and  $n = 3$  (red dashed lines) for fixed  $M_{BH,min} = 2 M_\star = 2$  TeV. The right panel shows  $M_\star = 1$  TeV (black solid lines) and  $M_\star = 5$  TeV (red dashed lines) for  $M_{BH,min} = 2 M_\star$  and  $n = 6$ .

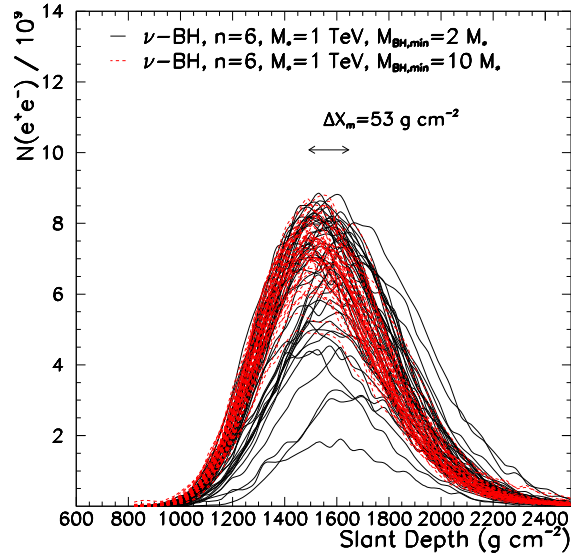


FIG. 9: Number of  $e^+e^-$  vs slant depth for BH-induced air showers with  $M_{BH,min} = 2 M_\star$  (black solid lines) and  $M_{BH,min} = 5 M_\star$  (red dashed lines) at fixed  $n = 6$  and  $M_\star = 1$  TeV.

## V. OTHER SIGNATURES OF BH FORMATION

In the previous sections we discussed the different characteristics of neutrino initiated air showers in the atmosphere for SM interactions compared to the formation of TeV BHs. Given the uncertainties in the BH formation, evaporation processes, and the inherent fluctuations of air showers, clear signals of BH formation are difficult to extract and require a large number of neutrino events. The problem is analogous to separating proton-induced air showers from gamma-ray air showers, but with an additional unknown  $X_0$ . If future experiments can observe both  $\Upsilon$  and  $\mu$ 's of a large number of neutrino air showers, a separation between SM and BH events could be reached. Given the low expected flux of ultrahigh energy neutrinos, hybrid observatories larger than Auger would be necessary.

As an alternative to a large study of neutrino induced air showers, BH fragmentation may be observable via a few events that have no significant background. For instance, the production of  $\tau$  leptons in BH evaporation have no significant counterpart in the SM air showers. The fragmentation of heavy BHs may allow multiple  $\tau$  production with  $\tau$  energies two or more orders of magnitude lower than the primary neutrino energy. This kind of process is strongly suppressed in SM interactions.

One effect of the lower energy of  $\tau$ 's produced in BH interactions versus the SM case is the shorter decay length of the generated  $\tau$ . As a concrete example, if a neutrino with energy  $E_\nu = 10^7$  TeV crosses the Andes mountains towards the Auger Observatory this neutrino-induced BH can produce one or more  $\tau$  leptons with energies around  $10^5$  TeV. These  $\tau$ 's would decay at a distance of about 5 km from the mountains where the Auger Observatory is located. A shower from one such  $\tau$  decay from the direction of the Andes would be surprising and even more so if two decays from that direction were to occur. If the same neutrino had a SM interaction it could create a single  $\tau$  with about  $2 \times 10^6$  TeV. This SM produced  $\tau$  will decay after traveling about 100 km, past the Auger Observatory.

This example illustrates that for a given neutrino flux and flavor content, the number of produced  $\tau$ 's may help separate rare events that have a BH origin versus a SM origin. Earth-skimming events [71, 73] would also show different energies for the generated  $\tau$ 's. A significant study of these signatures depends on detailed assumptions of the neutrino flux and the detector capabilities and will be more fully addressed elsewhere.

## VI. CONCLUSION

We considered the possibility of using UHECR observations to detect effects from TeV gravity theories. We focused our attention on the formation and fragmentation of BHs at TeV CM energies and found that distinguishing BH formation and SM air showers is much more challenging than previously expected.

The first challenge on this type of study is the unknown details of BH formation and fragmentation. The BH formation cross section has large uncertainties and varies by orders of magnitude with model parameters that include the number of extra dimensions, the energy scale of extra dimensions, and the minimum mass of BHs. In principle, contrasting the observed neutrino flux with the expected neutrino flux can help constrain the neutrino nucleon cross section, but the uncertainties of the BH cross section limit the translation of these constraints into constraints on TeV gravity parameters.

We showed that BH forming interactions generate very different air showers from SM interactions, but the inability of realistic detectors to observe the first interaction point hides most of the difference between these air showers. We proposed two parameters that show the different characteristics of the two types of air showers: the rise-depth and the muon content of the air showers. The BH air showers tend to rise faster, given their large multiplicity, and have larger muon contents, given their hadronic nature. A BH air shower is similar to a hadronic air shower that can occur at a much higher depth in the atmosphere, i.e., a very deeply penetrating hadronic air shower. Deeply penetrating SM air showers are dominated by CC processes that generate electromagnetic air showers. SM neutrino air showers are similar to deeply penetrating photon-showers. The rise-depth and the muon content can help distinguish these characteristics of the SM and BH types of air showers, but the process requires a large number of events to overcome the inherent fluctuations that generally occur from shower-to-shower. Given that present observatories are not large enough to study a large number of neutrino events, the kind of distinction we propose will not be achieved in the near future.

In addition to proposing the study of different air shower characteristics, we suggested that unique events can arise from BH formation which are suppressed in SM interactions, such as the multiple  $\tau$  generation. The rate for these events is low if the ultrahigh energy neutrino flux is at the level of the expected cosmogenic neutrinos. However, unusual air

showers from the direction of a mountain chain can signal both a larger flux of neutrinos and a departure from the SM interactions.

### Acknowledgments

We are grateful to Jaime Alvarez-Muniz, Luis Anchordoqui, Suyong Choi, Maria-Teresa Dova, Jonathan Feng, Haim Goldberg, and Al Shapere for useful discussion and comments. This work was supported in part by the NSF through grant AST-0071235 and DOE grant DE-FG0291-ER40606 at the University of Chicago and at the Center for Cosmological Physics by grant NSF PHY-0114422.

- 
- [1] I. Antoniadis, *Phys. Lett. B* **246**, 377 (1990).
  - [2] N. Arkani-Hamed, S. Dimopoulos and G. R. Dvali, *Phys. Lett. B* **429**, 263 (1998) [arXiv:hep-ph/9803315].
  - [3] I. Antoniadis, N. Arkani-Hamed, S. Dimopoulos and G. R. Dvali, *Phys. Lett. B* **436**, 257 (1998) [arXiv:hep-ph/9804398].
  - [4] L. Randall and R. Sundrum, *Phys. Rev. Lett.* **83**, 3370 (1999) [arXiv:hep-ph/9905221].
  - [5] L. Randall and R. Sundrum, *Phys. Rev. Lett.* **83**, 4690 (1999) [arXiv:hep-th/9906064].
  - [6] G. F. Giudice, R. Rattazzi and J. D. Wells, *Nucl. Phys. B* **544**, 3 (1999) [arXiv:hep-ph/9811291].
  - [7] T. Han, J. D. Lykken and R. J. Zhang, *Phys. Rev. D* **59**, 105006 (1999) [arXiv:hep-ph/9811350].
  - [8] J. L. Hewett, *Phys. Rev. Lett.* **82**, 4765 (1999) [arXiv:hep-ph/9811356].
  - [9] T. G. Rizzo, *Phys. Rev. D* **59**, 115010 (1999) [arXiv:hep-ph/9901209].
  - [10] G. F. Giudice and A. Strumia, arXiv:hep-ph/0301232.
  - [11] E. G. Adelberger [EOT-WASH Group Collaboration], arXiv:hep-ex/0202008.
  - [12] T. Banks and W. Fischler, arXiv:hep-th/9906038.
  - [13] E. J. Ahn, M. Cavaglià and A. V. Olinto, *Phys. Lett. B* **551**, 1 (2003) [arXiv:hep-th/0201042].
  - [14] E. J. Ahn and M. Cavaglià, *Gen. Rel. Grav.* **34**, 2037 (2002) [arXiv:hep-ph/0205168].
  - [15] S. Dimopoulos and R. Emparan, *Phys. Lett. B* **526**, 393 (2002) [arXiv:hep-ph/0108060].

- [16] K. Cheung, Phys. Rev. D **66**, 036007 (2002) [arXiv:hep-ph/0205033].
- [17] R. Casadio and B. Harms, Int. J. Mod. Phys. A **17**, 4635 (2002) [arXiv:hep-th/0110255].
- [18] M. Cavaglià, Int. J. Mod. Phys. A **18**, 1843 (2003) [arXiv:hep-ph/0210296].
- [19] H. Tu, arXiv:hep-ph/0205024.
- [20] G. Landsberg, arXiv:hep-ph/0211043.
- [21] R. Emparan, arXiv:hep-ph/0302226.
- [22] S. B. Giddings and S. Thomas, Phys. Rev. D **65**, 056010 (2002) [arXiv:hep-ph/0106219].
- [23] S. Dimopoulos and G. Landsberg, Phys. Rev. Lett. **87**, 161602 (2001) [arXiv:hep-ph/0106295].
- [24] K. Cheung, Phys. Rev. Lett. **88**, 221602 (2002) [arXiv:hep-ph/0110163].
- [25] I. Mocioiu, Y. Nara and I. Sarcevic, Phys. Lett. B **557**, 87 (2003) [arXiv:hep-ph/0301073].
- [26] J. L. Feng and A. D. Shapere, Phys. Rev. Lett. **88**, 021303 (2002) [arXiv:hep-ph/0109106].
- [27] L. A. Anchordoqui, J. L. Feng, H. Goldberg and A. D. Shapere, Phys. Rev. D **65**, 124027 (2002) [arXiv:hep-ph/0112247].
- [28] L. Anchordoqui and H. Goldberg, Phys. Rev. D **65**, 047502 (2002) [arXiv:hep-ph/0109242].
- [29] A. Ringwald and H. Tu, Phys. Lett. B **525**, 135 (2002) [arXiv:hep-ph/0111042].
- [30] L. Anchordoqui, T. Paul, S. Reucroft and J. Swain, arXiv:hep-ph/0206072.
- [31] S. I. Dutta, M. H. Reno and I. Sarcevic, Phys. Rev. D **66**, 033002 (2002) [arXiv:hep-ph/0204218].
- [32] M. Ave, J. A. Hinton, R. A. Vazquez, A. A. Watson and E. Zas, Phys. Rev. Lett. **85**, 2244 (2000) [arXiv:astro-ph/0007386].
- [33] V.S. Berezinsky and G.T. Zatsepin, Phys. Lett B **28**, 423 (1969).
- [34] V.S. Berezinsky and G.T. Zatsepin, Soviet Journal of Nuclear Physics **11**, 111 (1970).
- [35] K. Greisen, Phys. Rev. Lett. **16**, 748 (1966).
- [36] G. T. Zatsepin and V. A. Kuzmin, JETP Lett. **4**, 78 (1966) [Pisma Zh. Eksp. Teor. Fiz. **4**, 114 (1966)].
- [37] P. Bhattacharjee and G. Sigl, Phys. Rept. **327**, 109 (2000) [arXiv:astro-ph/9811011].
- [38] R. Engel, D. Seckel and T. Stanev, Phys. Rev. D **64**, 093010 (2001) [arXiv:astro-ph/0101216].
- [39] C. Tyler, A. V. Olinto and G. Sigl, Phys. Rev. D **63**, 055001 (2001) [arXiv:hep-ph/0002257].
- [40] T. Sjöstrand, P. Edén, C. Friberg, L. Lönnblad, G. Miu, S. Mrenna and E. Norrbin, Computer Physics Commun. **135** (2001) 238
- [41] S. J. Sciutto, arXiv:astro-ph/9905185.

- [42] R. Brock *et al.* [CTEQ Collaboration], *Rev. Mod. Phys.* **67**, 157 (1995).
- [43] J. Pumplin, D. R. Stump, J. Huston, H. L. Lai, P. Nadolsky and W. K. Tung, *JHEP* **0207**, 012 (2002) [arXiv:hep-ph/0201195].
- [44] R. Emparan, M. Masip and R. Rattazzi, *Phys. Rev. D* **65**, 064023 (2002) [arXiv:hep-ph/0109287].
- [45] R. Emparan, G. T. Horowitz and R. C. Myers, *Phys. Rev. Lett.* **85**, 499 (2000) [arXiv:hep-th/0003118].
- [46] M. Cavaglià, arXiv:hep-ph/0305256.
- [47] M. Cavaglià, S. Das and R. Maartens, *Class. Quant. Grav.* **20**, L205 (2003) [arXiv:hep-ph/0305223].
- [48] P. C. Argyres, S. Dimopoulos and J. March-Russell, *Phys. Lett. B* **441**, 96 (1998) [arXiv:hep-th/9808138].
- [49] T. Han, G. D. Kribs and B. McElrath, *Phys. Rev. Lett.* **90**, 031601 (2003) [arXiv:hep-ph/0207003].
- [50] L. Anchordoqui and H. Goldberg, *Phys. Rev. D* **67**, 064010 (2003) [arXiv:hep-ph/0209337].
- [51] D. N. Page, *Phys. Rev. D* **13**, 198 (1976).
- [52] P. Kanti and J. March-Russell, *Phys. Rev. D* **66**, 024023 (2002) [arXiv:hep-ph/0203223].
- [53] P. Kanti and J. March-Russell, arXiv:hep-ph/0212199.
- [54] S. C. Park, K. y. Oda and D. Ida, arXiv:hep-th/0212108.
- [55] V. Frolov and D. Stojkovic, *Phys. Rev. D* **66**, 084002 (2002) [arXiv:hep-th/0206046].
- [56] V. Frolov and D. Stojkovic, *Phys. Rev. Lett.* **89**, 151302 (2002) [arXiv:hep-th/0208102].
- [57] D. J. Bird *et al.* [HIRES Collaboration], *Phys. Rev. Lett.* **71**, 3401 (1993).
- [58] D. J. Bird *et al.*, *Astrophys. J.* **441**, 144 (1995).
- [59] T. Abu-Zayyad *et al.*, *Nucl. Instrum. Meth. A* **450**, 253 (2000).
- [60] *The Pierre Auger Project Design Report*. By Auger Collaboration. FERMILAB-PUB-96-024, Jan 1996. ([www.auger.org](http://www.auger.org)).
- [61] See <http://www.euso-misson.org/>
- [62] See <http://heawww.gsfc.nasa.gov/docs/gamcosray/hecr/OWL/>
- [63] L. D. Landau and I. Pomeranchuk, *Dokl. Akad. Nauk Ser. Fiz.* **92**, 535 (1953).
- [64] L. D. Landau and I. Pomeranchuk, *Dokl. Akad. Nauk Ser. Fiz.* **92**, 735 (1953).
- [65] A. B. Migdal, *Phys. Rev.* **103**, 1811 (1956).

- [66] A. B. Migdal, Sov. Phys. JETP **5**, 527 (1957).
- [67] F. A. Aharonian, B. L. Kanevsk, and V. A. Sahakian, J. Phys. G **17**, 199 (1991).
- [68] A. N. Cillis, H. Fanchiotti, C. A. Garcia Canal and S. J. Sciutto, Phys. Rev. D **59**, 113012 (1999) [arXiv:astro-ph/9809334].
- [69] K. S. Capelle, J. W. Cronin, G. Parente and E. Zas, Astropart. Phys. **8**, 321 (1998) [arXiv:astro-ph/9801313].
- [70] M. Ave, R. A. Vazquez, E. Zas, J. A. Hinton and A. A. Watson, Astropart. Phys. **14**, 109 (2000) [arXiv:astro-ph/0003011].
- [71] X. Bertou, P. Billoir, O. Deligny, C. Lachaud and A. Letessier-Selvon, Astropart. Phys. **17**, 183 (2002) [arXiv:astro-ph/0104452].
- [72] J. Knapp, D. Heck, S. J. Sciutto, M. T. Dova and M. Risse, Astropart. Phys. **19**, 77 (2003) [arXiv:astro-ph/0206414].
- [73] J. L. Feng, P. Fisher, F. Wilczek and T. M. Yu, Phys. Rev. Lett. **88**, 161102 (2002) [arXiv:hep-ph/0105067].